

Article

Stability Studies of Highly Active Cobalt Catalyst for the Ammonia Synthesis Process

Magdalena Zybert ^{1,*} , Hubert Ronduda ¹ , Wojciech Patkowski ¹ , Weronika Rybińska ¹,
Andrzej Ostrowski ¹ , Kamil Sobczak ²  and Wioletta Raróg-Pilecka ¹ 

¹ Faculty of Chemistry, Warsaw University of Technology, Noakowskiego 3, 00-664 Warsaw, Poland; hubert.ronduda.dokt@pw.edu.pl (H.R.); wojciech.patkowski@pw.edu.pl (W.P.); weronika.rybinska.stud@pw.edu.pl (W.R.); andrzej.ostrowski@pw.edu.pl (A.O.); wioletta.pilecka@pw.edu.pl (W.R.-P.)

² Biological and Chemical Research Centre, University of Warsaw, Żwirki i Wigury 101, 02-089 Warsaw, Poland; ksobczak@cncb.uw.edu.pl

* Correspondence: magdalena.zybert@pw.edu.pl

Abstract: Ammonia is currently considered a promising compound for the chemical storage of hydrogen and as an energy carrier. However, large-scale ammonia production is not possible without an active and stable catalyst enabling efficient, long-term work without the need for its replacement. In this paper, the extended stability studies of the highly active promoted cobalt catalyst for ammonia synthesis were carried out. The long-term activity measurements in NH₃ synthesis reaction under conditions close to the industrial ones (400–470 °C, 6.3 MPa, H₂/N₂ = 3) were compiled with the characterization of catalyst properties on different stages of its work using N₂ physisorption, XRPD, STEM-EDX, and H₂-TPD. The accelerated aging method was used to simulate the deterioration of catalyst performance during industrial operation. Textural and structural characteristics revealed that the tested catalyst is highly resistant to high temperatures. The lack of significant changes in the specific surface area, morphology of the catalyst particles, surface distribution of elements, and chemisorption properties of cobalt surface during long-term heating (436 h) at 600 °C suggests that stable operation of the catalyst is possible in an ammonia synthesis reactor in the temperature range of 400–470 °C without the risk of losing its beneficial catalytic properties over time. The decline in catalyst activity during the long-term stability test was less than 10%.

Keywords: ammonia synthesis; cobalt catalyst; stability; catalyst deactivation; accelerated aging



Citation: Zybert, M.; Ronduda, H.; Patkowski, W.; Rybińska, W.; Ostrowski, A.; Sobczak, K.; Raróg-Pilecka, W. Stability Studies of Highly Active Cobalt Catalyst for the Ammonia Synthesis Process. *Energies* **2023**, *16*, 7787. <https://doi.org/10.3390/en16237787>

Academic Editor: Claudio Mele

Received: 31 October 2023

Revised: 23 November 2023

Accepted: 25 November 2023

Published: 27 November 2023



Copyright: © 2023 by the authors. Licensee MDPI, Basel, Switzerland. This article is an open access article distributed under the terms and conditions of the Creative Commons Attribution (CC BY) license (<https://creativecommons.org/licenses/by/4.0/>).

1. Introduction

A substantial negative impact on the environment caused by the energy production from fossil fuels makes it necessary to look for new, clean, and effective energy sources. Nowadays, hydrogen is considered the most environmentally friendly fuel [1–3]. Currently, hydrogen is mainly produced from methane by steam reforming with only a small contribution from other more sustainable technologies such as water electrolysis [3–7]. Steam reforming of methane is a mature technology and, at the same time, the least expensive for large-scale hydrogen production, which is mainly used for ammonia production and petroleum refining. These two processes account for about 82% of the total industrial hydrogen demand [8,9]. For other applications, the transport and storage of hydrogen is required, which is an extremely challenging issue due to its specific properties, e.g., a very high energy density by mass, a very low energy density by volume, diffusion through the materials, wide flammability limit ranges with both air and oxygen, and low boiling point (−252.9 °C). Hence, an interesting solution seems to be chemical storage, when hydrogen is bonded in molecules such as methanol, methane, metal amine salts (e.g., Mg(NH₃)₆Cl₂), ammonia, or hydrides (e.g., LiH, NaH, KH, LiBH₄, NaBH₄), which can be easily transported and decomposed on demand, giving hydrogen [10,11]. Among

them, one of the most promising compounds is ammonia, containing 17.6% hydrogen by weight, having high energy density per unit volume and acting as a green fuel due to the absence of carbon content, resulting in zero greenhouse gas emissions during combustion. Ammonia also has a significantly higher boiling point ($-33.8\text{ }^{\circ}\text{C}$) than hydrogen, making its storage and transportation relatively much easier than hydrogen [12]. So far, ammonia has been studied as a potential fuel for internal combustion engines, gas turbines, and other industrial purposes [12–15]. Ammonia production technology has been well developed for many years, and consolidated infrastructures for ammonia transport and storage already exist. Nevertheless, the research efforts toward new methods for ammonia synthesis as an alternative to the Haber–Bosch process are being made [16].

Large-scale ammonia production is not possible without the presence of a catalyst. Nowadays, when the efficient utilization of raw materials and energy is of utmost importance, it is desirable to modernize existing processes in order to extend the time of their operation. Hence, the stability of the catalyst, ensuring its long-term operation, is, next to the activity, one of the most crucial parameters characterizing the catalyst. Long-term, stable operation of the catalyst, without the need for its replacement, reducing the cost of plant shutdown, is the key factor qualifying it for industrial use. Numerous chemical and physical factors influence catalyst stability, resulting in deactivation [17]. Deactivation of the catalyst is inevitable, but its time varies significantly for the different processes (e.g., seconds for the cracking catalyst, months or a year for the hydrodesulfurization catalyst, or even 15 years for the iron ammonia synthesis catalyst). Deactivation can manifest itself mostly by changes in activity and selectivity over time. The most important causes of the catalyst deactivation include (1) poisoning, (2) fouling, (3) thermal degradation, (4) mechanical deactivation, and (5) corrosion/leaching [18–22]. Some of these mechanisms are chemical in nature and some are mechanical. However, it should be remembered that deactivation is a complex phenomenon, and the causes are often not independent. Moreover, it can occur at different levels, i.e., for specific active sites, catalyst particles, or even for the whole catalytic bed. Some deactivation mechanisms are reversible, and catalysts can often be regenerated before they ultimately have to be replaced. In some cases, damage is permanent and must be prevented or mitigated at least to maintain the catalyst lifetime, which is of crucial importance for the economics of a process. A catalyst deactivation generates costs connected not only with the replacement of catalyst charge but also with increasing raw materials and energy usage, cost of plant shutdown, lost production, and environmental costs of waste catalyst disposal. Studies of the catalyst's stability are required to predict the expected catalyst's lifetime in the plant and its optimization [23].

Although the definition of catalyst suggests that a catalyst can be used forever, it cannot be true in real industrial conditions due to numerous chemical and physical factors gradually decreasing activity/selectivity with the running time up to a certain value, qualifying it as inactive. In general, catalyst deactivation can be investigated by measuring activity as a function of time. However, some techniques are applicable only for industrial research because it is difficult to create conditions close to the industrial ones in a lab-scale study. This applies primarily to processes carried out in severe temperature and pressure conditions, and the catalyst's lifetime is strictly dependent on these conditions. In addition, reliable validation of catalyst stability requires monitoring activity changes over a long period of time. For academic research, the accelerated aging method based on applying high temperatures and/or high concentrations of poisons is useful to simulate the deterioration of catalyst performance under industrial conditions and achieve similar catalyst deactivation in a substantially shorter time [24]. The reliability of this method strongly depends on test conditions, which should differ as little as possible from those of the industrial reactor, except for one parameter chosen to give the acceleration (e.g., temperature) [25]. This methodology is commonly applied for thermal stability tests of most heterogeneous catalysts.

The iron catalyst for ammonia synthesis is a good representative of a catalyst in which activity is affected by thermal deactivation (slow sintering) when working in modern plants,

where feed gas purification is very effective, thus minimizing the effects of poisoning. For example, stability studies for this catalyst were conducted by Liu et al. [26], who subjected the commercial iron catalyst (A301) based on wustite to a heat-resistance stability test at 500 °C for 20 h (5 MPa, 30,000 h⁻¹), demonstrating the high stability of this catalyst. The loss of the ammonia concentration in the outlet gas was not higher than 0.5% and comparable to other iron catalysts based on magnetite. A similar procedure for wustite-based and magnetite-based catalysts was used by Pernicone et al. [27]. After the treatment at 600 °C for 16 h in synthesis gas (3 MPa, 20,000 h⁻¹), both studied catalysts retained about 80% of their initial activity. In the case of Ru catalysts, Lin et al. [28] performed the stability test of carbon-supported Ru catalysts by a high-temperature treatment process at 500 °C for 40 h. The results indicated a significant decrease in the ammonia synthesis rates for K-Ru/C and Ba-K-Ru/C by about 37% and 29%, respectively, compared to the initial rate. In the paper of Kowalczyk et al. [29], the short-term overheating of carbon-supported Ru catalysts at 520 °C for 24 h in 3H₂ + N₂ mixture was carried out. A threefold decrease in activity was observed for the K + Ru/C catalyst. However, the Ba + Ru/C catalyst was revealed to be strongly resistant to overheating—only a several percent decrease in the reaction rate was observed compared to the initial rate.

In our previous published papers [30–32], a detailed investigation was conducted to evaluate the catalytic performance and characteristics of the cobalt catalyst promoted with cerium and barium (CoCeBa). The studies revealed that the catalyst is highly active in ammonia synthesis under conditions close to the industrial ones. The activity of the CoCeBa catalyst was higher than that of the commercial iron catalyst (KM I, H. Topsoe) [30,31]. Moreover, the kinetic characteristics of the catalyst showed that it is much less sensitive to the ammonia content in the gas, especially at high ammonia content [31], than the iron catalyst. The present study is the continuation of our systematic studies on the CoCeBa catalyst and investigates the stability of this catalyst. The long-term activity in ammonia synthesis was analyzed with additional measurements characterizing the most important properties of the catalyst and their changes during long-term operation to understand better the changes occurring in this catalyst structure and the adsorption properties of its surface. Three samples of the CoCeBa catalyst were tested, in which the promoter (Ba) was introduced using three different preparative methods: deposition–precipitation, wet impregnation, and wet mixing. An additional aim of the work was to determine the influence of the promoter addition method on the properties and stability of the CoCeBa catalyst.

2. Materials and Methods

2.1. Catalyst Preparation

The mixture of cobalt carbonate and cerium carbonate in a fixed proportion was obtained by co-precipitation method using cobalt(II) nitrate hexahydrate and cerium(III) nitrate hexahydrate as Co and Ce sources and potassium carbonate as a precipitating agent. All the reagents used were of analytical grade. After drying at 120 °C and calcination at 500 °C of the precipitate, the mixture of Co₃O₄ and CeO₂ was obtained. A detailed description of the preparation method used can be found in our previous paper [31]. The obtained oxide mixture was then subjected to further procedures aiming to introduce the Ba promoter using three different preparative methods:

- (1) Wet impregnation (WI)—the material was impregnated with an appropriate amount of an aqueous solution of barium(II) nitrate. The solvent (water) was removed using a vacuum evaporator. Then, the sample was dried in air at 120 °C for 18 h.
- (2) Wet mixing (WM)—the material was mechanically mixed in a mortar with an appropriate amount of an aqueous solution of barium(II) nitrate and dried in air at 120 °C for 18 h.
- (3) Deposition–precipitation (DP)—the material was dispersed in an appropriate amount of an aqueous solution of barium(II) nitrate. Then, an aqueous solution of potassium carbonate was introduced dropwise and, maintaining a constant temperature (90 °C)

and stirring speed (350 rpm), the process of precipitation of barium carbonate on particles of a mixture of cobalt and cerium oxides was carried out. The precipitate was then filtered, washed, and dried at 120 °C for 18 h.

Finally, the samples were crushed and sieved to obtain grains of 0.20–0.63 mm in size. The obtained catalyst precursor samples were denoted as WI, WM, and DP, indicating the method of Ba promoter addition. The chemical composition of the prepared samples is indicated in Table 1. The method of Ba promoter addition caused the differences in textural properties and phase composition of the obtained catalyst precursors. A description of these properties of the catalyst precursors can be found in Table S1, Figures S1–S3.

Table 1. Physicochemical properties of the studied catalysts.

Catalyst	Element Content (wt%) ¹			SSA _{red} (m ² g ⁻¹) ²	
	Co	Ce	Ba	After Reduction in H ₂ Flow at 550 °C for 10 h	After Overheating in H ₂ Flow at 600 °C for 10/20/30 h
WI	70.1	8.4	12.6	5.6	3.9/4.2/3.7
WM	70.3	8.2	12.8	13.3	7.2/8.0/6.0
DP	70.7	8.1	12.3	11.2	11.8/12.3/10.4

¹ Element content determined using the XRF method. ² SSA_{red}—specific surface area determined for the reduced catalysts after heat treatment in H₂ flow at 550 or 600 °C based on the BET adsorption model.

2.2. Catalyst Characterization Methods

N₂ physisorption at −196 °C using an ASAP2020 instrument (Micromeritics Instrument Co., Norcross, GA, USA) was applied to determine the specific surface area (SSA) of the catalyst precursors and the reduced form of the catalysts (SSA_{red}). Prior to the measurements, each precursor sample (500 mg) was subjected to a two-step degassing procedure in a vacuum: at 90 °C for 1 h and then at 150 °C for 4 h. Before the measurement of the catalysts in reduced form, the catalyst sample was firstly reduced in situ at 550 °C for 10 h in H₂ flow and then subjected to degassing at 150 °C for 2 h. After the measurement, the same sample was reduced in situ at 600 °C for 10 h, degassed at 150 °C for 2 h, and the measurement was carried out. The same procedure was repeated after the further in situ reduction at 600 °C for 20 and 30 h. The reduction and degassing were conducted in the apparatus directly before N₂ physisorption measurements. The obtained data were approximated using the Brunauer–Emmett–Teller (BET) isotherm model in the relative pressure range (P/P₀) from 0.05 to 0.3, and the specific surface area (SSA and SSA_{red}) values were determined.

Powder X-ray diffraction patterns were recorded using a Bruker D8 Advance diffractometer (Bruker AXS, Karlsruhe, Germany) equipped with a LYNXEYE position-sensitive detector, using Cu-K α radiation ($\lambda = 0.15418$ nm). The data were collected in the Bragg–Brentano (θ/θ) horizontal geometry for the range $2\theta = 10$ – 80° in a continuous scan using 0.03° steps of 10 s/step. Data were collected under standard laboratory conditions.

TEM investigations were performed on a Talos F200X (FEI Company, Hillsboro, OR, USA) microscope operated at 200 kV. The measurements were performed in TEM and scanning TEM (STEM) modes using a high-angle annular dark-field (HAADF) detector and energy-dispersive X-ray spectroscopy on a Bruker BD4 spectrometer. The catalyst samples were investigated after ex situ reduction at 550 °C for 18 h under H₂ flow and after ex situ reduction at 600 °C for 96 h under H₂ flow.

H₂ temperature-programmed desorption using an AutoChem II 2920 instrument (Micromeritics Instrument Co., Norcross, GA, USA) was applied to determine the sorption properties of the catalyst surface. Before the analysis, the precursor sample (500 mg) was reduced in situ at 550 °C for 18 h under H₂ flow and purged at 570 °C for 2 h under Ar flow. Next, the system was cooled to 150 °C, and H₂ was introduced for 15 min. Then, the reactor was cooled to 0 °C and kept at that temperature for 15 min. Next, the sample was

purged with Ar at 0 °C until the baseline was stable. Desorption of hydrogen was carried out under Ar flow with a heating rate of 5 °C min⁻¹ up to 600 °C. A TCD detector was used to collect the data continuously during the process. The same experiments according to the procedure described above (i.e., hydrogen sorption and subsequent desorption) were conducted after reduction of the catalyst sample under H₂ flow at 600 °C for 18, 30, 66, 84, and 96 h.

2.3. Catalyst Activity and Stability Tests

The performance of the studied catalysts was tested in the NH₃ synthesis reaction. A high-pressure apparatus with a tubular flow reactor was used. Before the measurements, each catalyst sample (500 mg, grain size 0.2–0.63 mm) was subjected to an activation (reduction) procedure in a flow of a stoichiometric H₂/N₂ mixture (gas purity 99.99995 vol%, gas flow rate 30 dm³ h⁻¹) under the pressure of 0.1 MPa according to the following temperature program: 470 °C for 72 h → 520 °C for 24 h → 550 °C for 48 h. Next, the measurements of ammonia synthesis reaction rate over the catalyst were conducted under steady-state conditions, i.e., 6.3 MPa, 400–470 °C, H₂/N₂ = 3, gas flow rate 70 dm³ h⁻¹. NH₃ concentration in the outlet gas was determined using an interferometer, and NH₃ synthesis reaction rate was calculated. A detailed description of the experimental setup and calculating methods can be found in [33]. To investigate the stability of the catalyst, the overheating procedure was applied. The catalysts' heat treatment conditions were as follows: 600 °C, 0.1 MPa, H₂/N₂ = 3, gas flow rate 30 dm³ h⁻¹. The long-term heat treatment was carried out for a total time of 436 h. Catalyst activity measurements were conducted under steady-state conditions, i.e., 6.3 MPa, 400 °C, H₂/N₂ = 3, gas flow rate 70 dm³ h⁻¹ after 16, 82, 98, 266, and 436 h of overheating.

3. Results

3.1. Evaluation of Catalyst Stability in Ammonia Synthesis Reaction

The performance of CoCeBa catalysts in ammonia synthesis was systematically examined as a function of time. All the studied catalysts displayed high initial activity (after standard reduction at 550 °C) in the ammonia synthesis reaction, presented as unfilled marks in Figure 1a. The promoter (Ba) addition method appears to have a slight effect on the activity of the catalysts—the difference in reaction rates resulting from various promoter addition methods ranged from 10 to 25%. The CoCeBa catalyst obtained using the deposition–precipitation method (DP sample) exhibited the highest activity among the studied catalytic systems. Since the accelerated aging method is most appropriate to evaluate the stability of the catalyst on the laboratory scale, a high-temperature treatment at 600 °C for a total time of 436 h was carried out to simulate the deterioration of catalyst performance under industrial conditions. As shown in Figure 1a, the catalytic activities initially increased by approximately 10% for all the catalysts after the first 16 h of treatment at 600 °C compared to the activity after activation. This may be related to the progressive reduction process of the catalysts, connected with the production of an additional promoter (BaCeO₃) with strong electron-donating properties, favoring the high activity of the tested catalysts in the ammonia synthesis reaction. The influence of this promoter on CoCeBa catalyst activity and its formation during catalyst reduction was described in detail in our previous paper [32]. The further heating of the catalysts at 600 °C for the next 66 h caused the activity of the DP and WI catalysts to decrease slightly (by 8 and 6%, respectively) or remained unchanged for the WM catalyst. The long-term stability test was continued for a total time of 436 h (over 18 days), and no further changes in the activity of CoCeBa catalysts were observed during their operation. The obtained results evidence that the CoCeBa catalyst is strongly resistant to overheating. This allows us to assume that this type of catalyst can operate stably and effectively even at temperatures higher than the standard operating temperature of ammonia synthesis reactors. Figure 1b presents the temperature dependence of the ammonia synthesis rate of the CoCeBa catalysts at the end of the long-term stability test. The studied catalysts exhibited similar activity across the examined

temperature range of 400–470 °C. The apparent activation energies determined from the slopes of the Arrhenius plots (Figure S4) were similar and in the range of 47–49 kJ mol⁻¹.

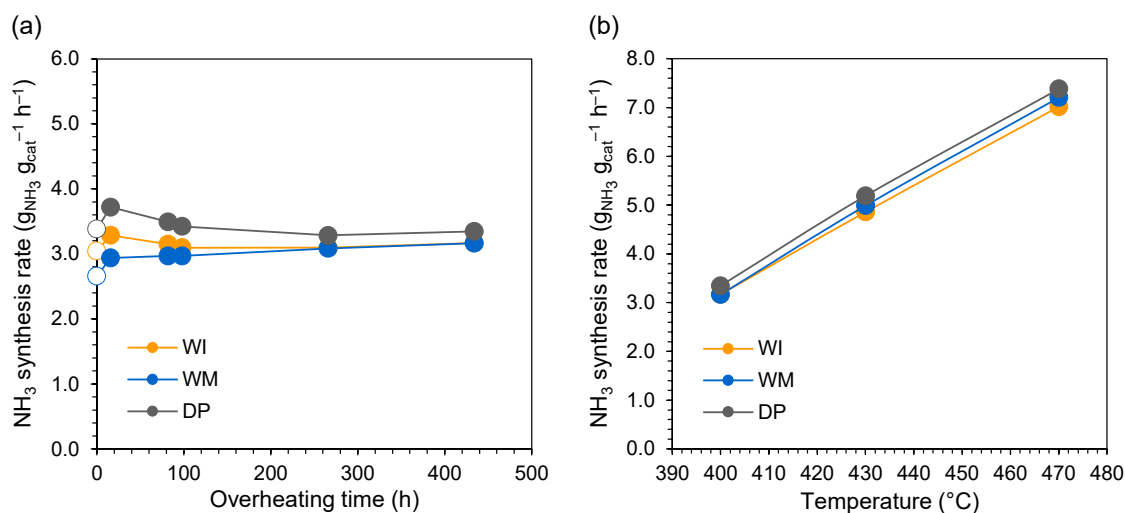


Figure 1. (a) Ammonia synthesis rate as a function of overheating time (reaction conditions: 400 °C, 6.3 MPa, H₂/N₂ = 3, 70 dm³ h⁻¹; heat treatment conditions: 600 °C, 0.1 MPa, H₂/N₂ = 3, 30 dm³ h⁻¹). Unfilled marks—activity after standard activation (reduction) at a temperature of 550 °C, filled marks—activity after heat treatment at a temperature of 600 °C. (b) Temperature dependence of the ammonia synthesis rate at 6.3 MPa, H₂/N₂ = 3, 70 dm³ h⁻¹ after long-term heat treatment at 600 °C for 436 h.

The superior performance of the CoCeBa catalysts for ammonia synthesis was revealed by comparison to the literature results with similar reaction conditions (Table S2) [34–40]. In particular, the ammonia formation rate over CoCeBa catalysts reached 3.17–3.35 g_{NH₃} g_{cat}⁻¹ h⁻¹, which was almost three times that of commercial iron catalyst (ZA-5). In addition, the CoCeBa catalysts showed much higher activity than similar composite catalysts (Table S2).

3.2. Evaluation of Catalyst Properties during Stability Studies

To explain the effect of the high stability of the CoCeBa catalyst during the long-term stability test, detailed characterization studies were performed focusing on changes in structural and sorption properties of the catalyst surface during the long-term operation.

Firstly, N₂ physisorption analysis of the specific surface area of the catalysts (SSA_{red}) was carried out during long-term heat treatment in the H₂ flow (in situ measurements). As shown in Table 1, the initial values of the SSA_{red} parameter after reduction in the hydrogen flow at a temperature of 550 °C for 10 h were in the range of 5–13 m² g⁻¹, depending on the catalyst preparation method. As a result of overheating of the catalysts in the hydrogen flow at a temperature of 600 °C for 10 h, a decrease in the specific surface area was observed by 30 and 45% for the WI and WM samples, respectively. For the DP catalyst, no change in the SSA_{red} value was observed. Further overheating under these conditions for 20 and 30 h did not cause any further changes in the specific surface area of the studied catalysts. This indicates a high resistance to the sintering of the studied catalysts.

Next, the structure of the CoCeBa catalysts at various stages of their operation was investigated using XRPD (ex situ measurements). The main phases identified in the tested catalysts are marked in Figure 2. It is clearly visible that regardless of the composition of the catalyst precursors, resulting directly from the method used to introduce the Ba promoter (Figure S3), the catalysts in the active form, i.e., after reduction in hydrogen flow at 550 °C for 18 h, showed a similar phase composition (Figure 2). For all catalysts, the presence of two metallic cobalt phases (hexagonal and cubic) was observed. However, for catalysts obtained using impregnation methods (WM, WI samples), the reflections of two crystalline forms of cobalt (hexagonal Co and cubic Co) were observed. Meanwhile, for the catalyst

obtained using the deposition–precipitation method (DP sample), only reflections from the cubic Co were observed. Moreover, barium cerate (BaCeO_3) phase was identified for all the studied catalysts. This phase formed in situ under the conditions of catalyst reduction as a result of the interaction of components containing Ce and Ba. A detailed investigation of the in situ formation of BaCeO_3 promoter during the studied catalyst reduction can be found in our previous paper [32].

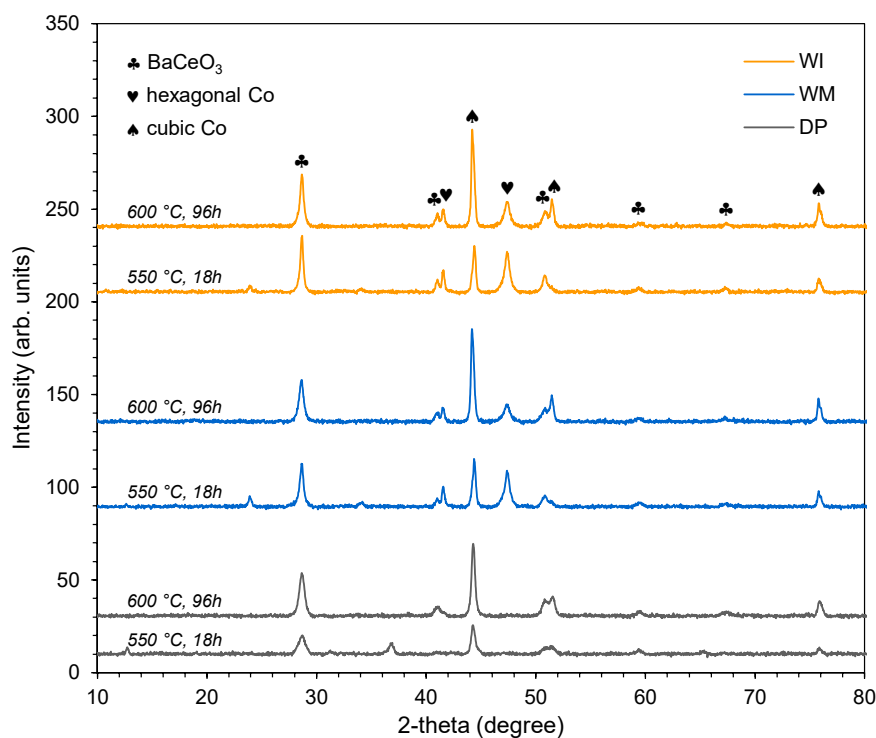


Figure 2. Diffractograms of the CoCeBa catalysts after reduction in hydrogen flow at 550 °C for 18 h and after overheating in hydrogen flow at 600 °C for 96 h.

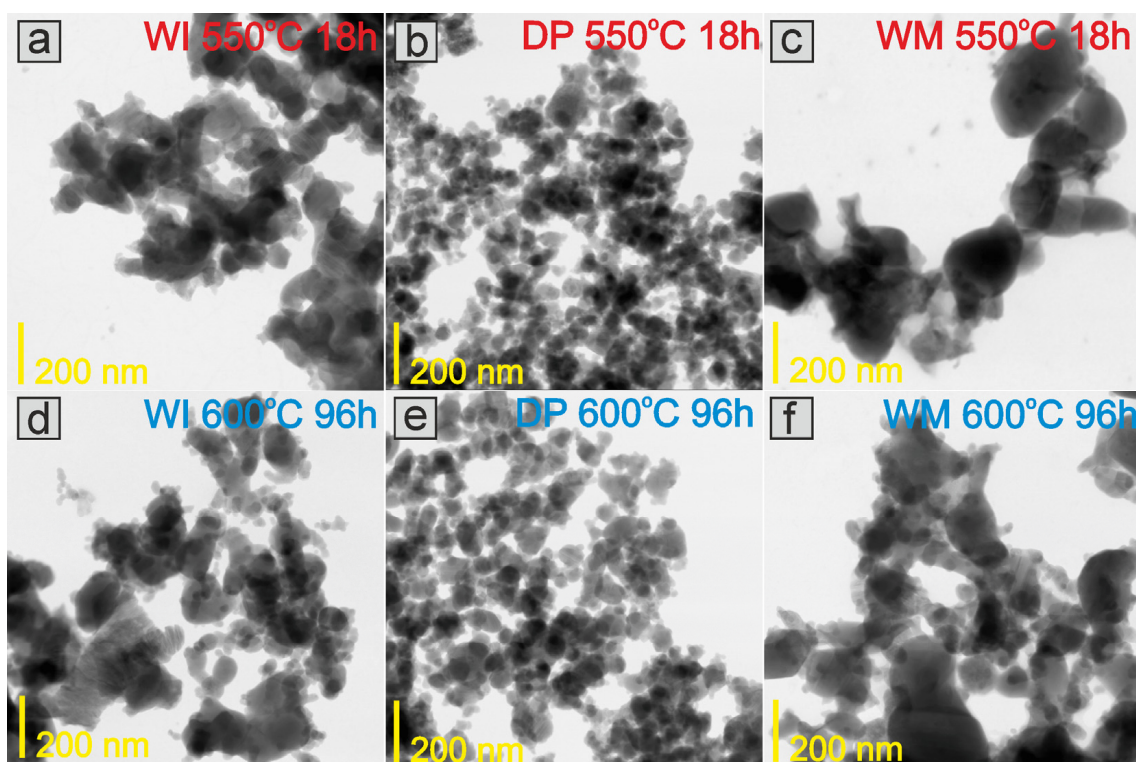
After overheating the catalysts in hydrogen flow at a temperature of 600 °C for 96 h, no significant changes in the phase composition of the catalysts were observed (Figure 2). The main components of the catalyst were still cubic Co, hexagonal Co, and BaCeO_3 . However, only reflections from the cubic Co were observed for the catalyst obtained using the deposition–precipitation method (DP sample). In turn, for the catalysts obtained using impregnation methods (WI, WM samples), the intensity of reflections derived from hexagonal Co decreased while the intensity of reflections from cubic Co increased. This may be related to the phase transformation of hexagonal cobalt (hcp) into cubic cobalt (fcc) during high-temperature heating of the catalyst [41–43]. However, changes in the amount of hexagonal Co and cubic Co phases did not significantly influence the size of the Co crystallites (Table 2). After reduction at 550 °C for 18 h, the crystallites of the active phase had a size in the range of 15–17 nm and 20–26 nm for the hexagonal Co and cubic Co phases, respectively. After overheating at a temperature of 600 °C for 96 h, the Co crystallite sizes were in the range of 15–17 nm and 23–27 nm for the hexagonal Co and cubic Co phases, respectively. Moreover, after overheating the catalysts at 600 °C, it was observed that the reflections from the BaCeO_3 promoter phase became more intense, indicating increasing crystallinity of this phase. The average BaCeO_3 crystallite sizes in the CoCeBa catalysts after overheating at 600 °C were larger than those after heating at 550 °C (Table S2). At the same time, there were no significant differences in the unit cell parameters of the BaCeO_3 phases in the CoCeBa catalysts before and after overheating.

Table 2. Average Co crystallite size calculated based on the FWHM value obtained by Rietveld refinement method.

Catalyst	After Reduction in H ₂ Flow at 550 °C for 18 h		After Overheating in H ₂ Flow at 600 °C for 96 h	
	Hexagonal Co (nm)	Cubic Co (nm)	Hexagonal Co (nm)	Cubic Co (nm)
WI	15	26	17	27
WM	17	25	15	26
DP	–	20	–	23

Small reflections, visible on the diffraction profiles after reduction at 550 °C in the range of the 2-theta = 11–36°, disappeared. They were most likely related to the presence of barium carbonate, which, during long-term overheating in hydrogen, reacted with the second promoter (cerium oxide), resulting in the BaCeO₃ phase (in situ formation of the promoter phase) [32].

Microscopic investigations were performed for the catalysts at various stages of the long-term stability test (ex situ measurements) to analyze the morphology and chemical composition of the surface layers of the prepared catalysts. The representative TEM images of the CoCeBa catalysts after reduction in hydrogen flow at 550 °C for 18 h presented in Figure 3 clearly indicate the difference in their morphology depending on the method of the promoter addition. The catalysts obtained using wet impregnation (Figure 3a) and the wet mixing method (Figure 3c) consist of agglomerates with irregular shapes containing grains of different sizes but smaller than 100 nm and 200 nm, respectively. The morphology of the catalyst obtained using the deposition–precipitation method (DP) seems to be different. Figure 3b indicates the significant homogeneity of this catalyst. The DP catalyst particles are characterized by regular shapes of small sizes below 50 nm.

**Figure 3.** TEM images of the studied WI (a,d), DP (b,e), and WM (c,f) catalysts after reduction in hydrogen flow at 550 °C for 18 h and after overheating in H₂ flow at 600 °C for 96 h (ex situ measurements).

The morphology does not change after overheating the catalysts in H_2 flow at $600\text{ }^\circ\text{C}$ for 96 h (Figure 3d–f). This lack of macroscopic changes in the catalysts' morphology proves that the particles are highly resistant to overheating and that there are no sintering effects that could negatively affect the long-term performance of catalysts in the ammonia synthesis reactor. STEM-EDX analysis provided additional information on the chemical composition of the catalysts' surface. It is clearly visible in the EDX maps presented in Figures 4a, 5a and 6a that after reduction in hydrogen flow at $550\text{ }^\circ\text{C}$ for 18 h, the homogeneous distribution of Co throughout the catalysts particles was observed for all the studied samples regardless of the promoter addition method used. The distribution maps for cerium, barium, and oxygen indicate that the $BaCeO_3$ promoter is evenly distributed throughout the samples. It does not form separate grains but is relatively well distributed on the surface of the cobalt particles. Only a few areas of greater promoter concentration can be found on the studied catalyst surfaces. After overheating the catalysts in H_2 flow at $600\text{ }^\circ\text{C}$ for 96 h, the distribution of the catalyst components remains rather unchanged (Figures 4b, 5b and 6b). This favorable element distribution may promote effective electron donation from the promoter to the active phase, ensuring its efficient catalytic performance during long-term operation [44].

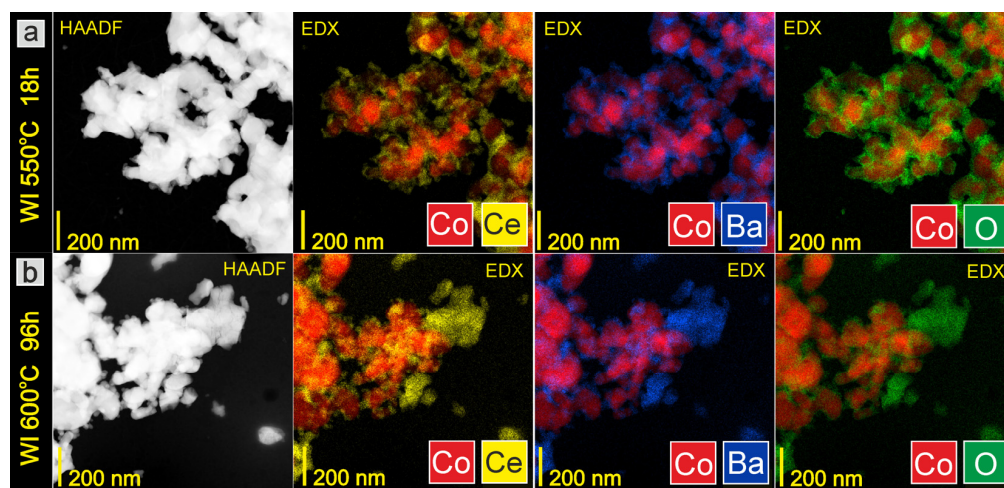


Figure 4. STEM-HAADF images and corresponding EDX distribution maps of elements for WI catalyst: (a) after reduction in hydrogen flow at $550\text{ }^\circ\text{C}$ for 18 h, (b) after overheating in hydrogen flow at $600\text{ }^\circ\text{C}$ for 96 h (ex situ measurements).

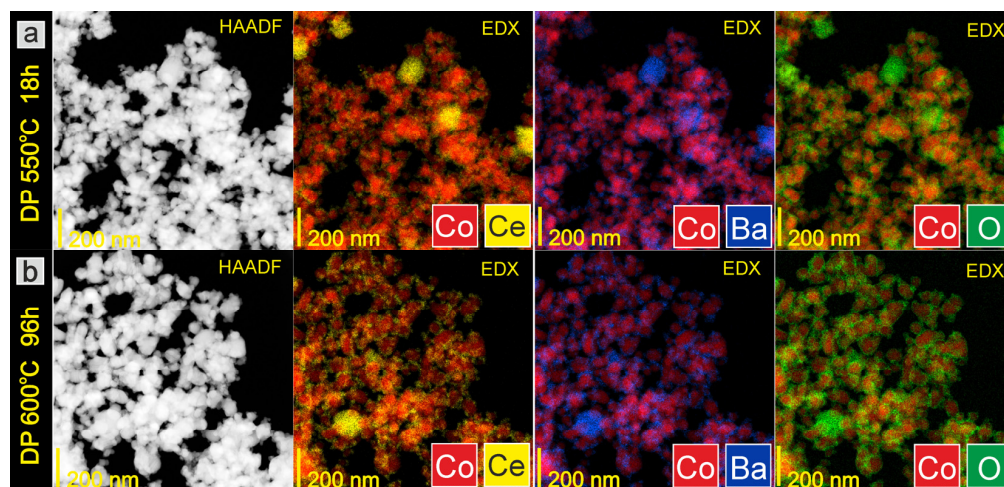


Figure 5. STEM-HAADF images and corresponding EDX distribution maps of elements for DP catalyst: (a) after reduction in hydrogen flow at $550\text{ }^\circ\text{C}$ for 18 h, (b) after overheating in hydrogen flow at $600\text{ }^\circ\text{C}$ for 96 h (ex situ measurements).

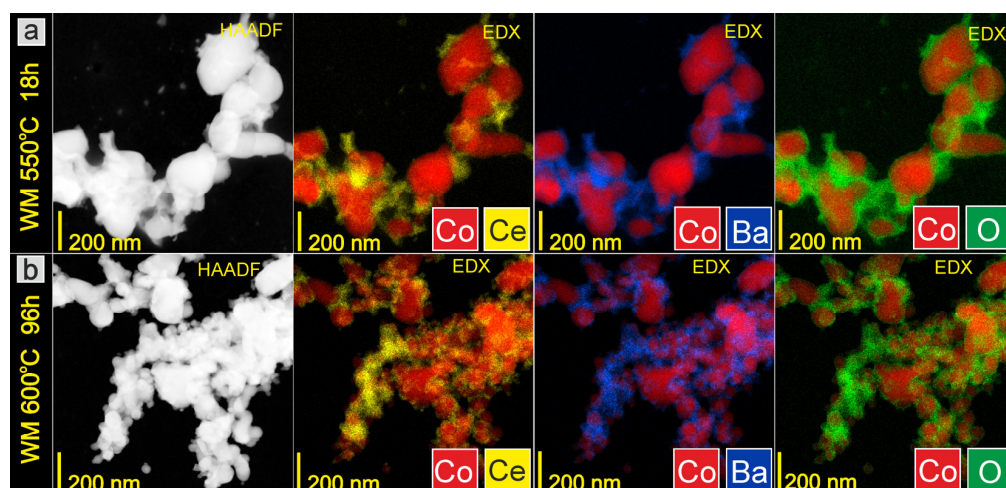


Figure 6. STEM-HAADF images and corresponding EDX distribution maps of elements for WM catalyst: (a) after reduction in hydrogen flow at 550 °C for 18 h, (b) after overheating in hydrogen flow at 600 °C for 96 h (ex situ measurements).

The adsorption properties of the catalysts' surface were examined using H_2 -TPD experiments. Although nitrogen dissociation is considered the rate-determining step of the ammonia synthesis reaction [45–49], the strong chemisorption of the second reactant, i.e., hydrogen, on the catalyst surface may also be an essential factor determining the operation of the catalyst. In particular, strong chemisorption of hydrogen on the catalyst surface, known as the “hydrogen poisoning” phenomenon, may cause the catalyst's low efficiency or rapid performance degradation during long-term operation. Hence, the obtained results in the form of hydrogen desorption curves from the surfaces of the studied catalysts (Figure 7a–c) allowed for the interpretation of the strength of active sites binding hydrogen to the catalyst surface, which is of pivotal importance from the point of view of the mechanism of NH_3 synthesis reaction.

Figure 7a shows the H_2 -TPD profiles of the catalyst obtained by wet impregnation (WI sample). After reduction in hydrogen flow at 550 °C for 18 h, two desorption peaks are observed for the WI catalyst in the temperature range of 0–600 °C. The low-temperature (<200 °C) and high-temperature (400–550 °C) desorption peaks can be ascribed to the cobalt active sites that weakly and strongly bind hydrogen, respectively [50,51]. The area ratio of low-to-high-temperature peaks is about 0.6, which means that the sites binding hydrogen strongly to the catalyst surface dominate in the WI catalyst. However, hydrogen desorption from strongly binding sites occurs in a temperature range similar to that in which the ammonia synthesis reaction is carried out. It can, therefore, be concluded that all adsorption sites identified for the WI catalyst are available to the reagents under the reaction conditions [50]. This means the catalyst is free of hydrogen poisoning under the tested conditions. After overheating in hydrogen flow at 600 °C for 18 h, the desorption profile did not change, i.e., the nature of the adsorption sites was preserved. Only the intensity of the low-temperature peak decreased slightly, i.e., the ratio of low-to-high-temperature peaks decreased to 0.4. It should be underlined that no further changes in the hydrogen desorption profile from the surface of this catalyst were observed during further overheating of the catalyst for 30, 66, 84, and 96 h. Similar hydrogen desorption profiles (Figure 7b) were observed for the catalyst obtained using the wet mixing method (WM sample) both after reduction in hydrogen flow at 550 °C for 18 h and after overheating at 600 °C. The temperature ranges for hydrogen desorption for each type of active site were similar to that for the WI catalyst. Only the low-to-high-temperature peak ratio was slightly higher and reached ca. 1.0 after reduction at 550 °C and 0.7 after overheating at 600 °C. Therefore, it is clear that in the case of the WM catalyst, similarly to the WI catalyst, the active sites strongly binding hydrogen on the catalyst surface play a dominant role. A different distribution of adsorption sites was observed for the catalyst obtained

using the deposition–precipitation method (DP sample) (Figure 7c). After reduction at 550 °C, the desorption profile consists of a significant low-temperature peak in the range of 0–300 °C and a broad high-temperature peak of very low intensity in the temperature range of 400–600 °C. This indicates the dominance of weakly hydrogen-binding sites on the surface of the DP catalyst. After overheating at 600 °C for 18 h, the high-temperature peak disappeared completely, and the desorption profile did not change further during overheating at 600 °C for 30, 66, 84, and 96 h.

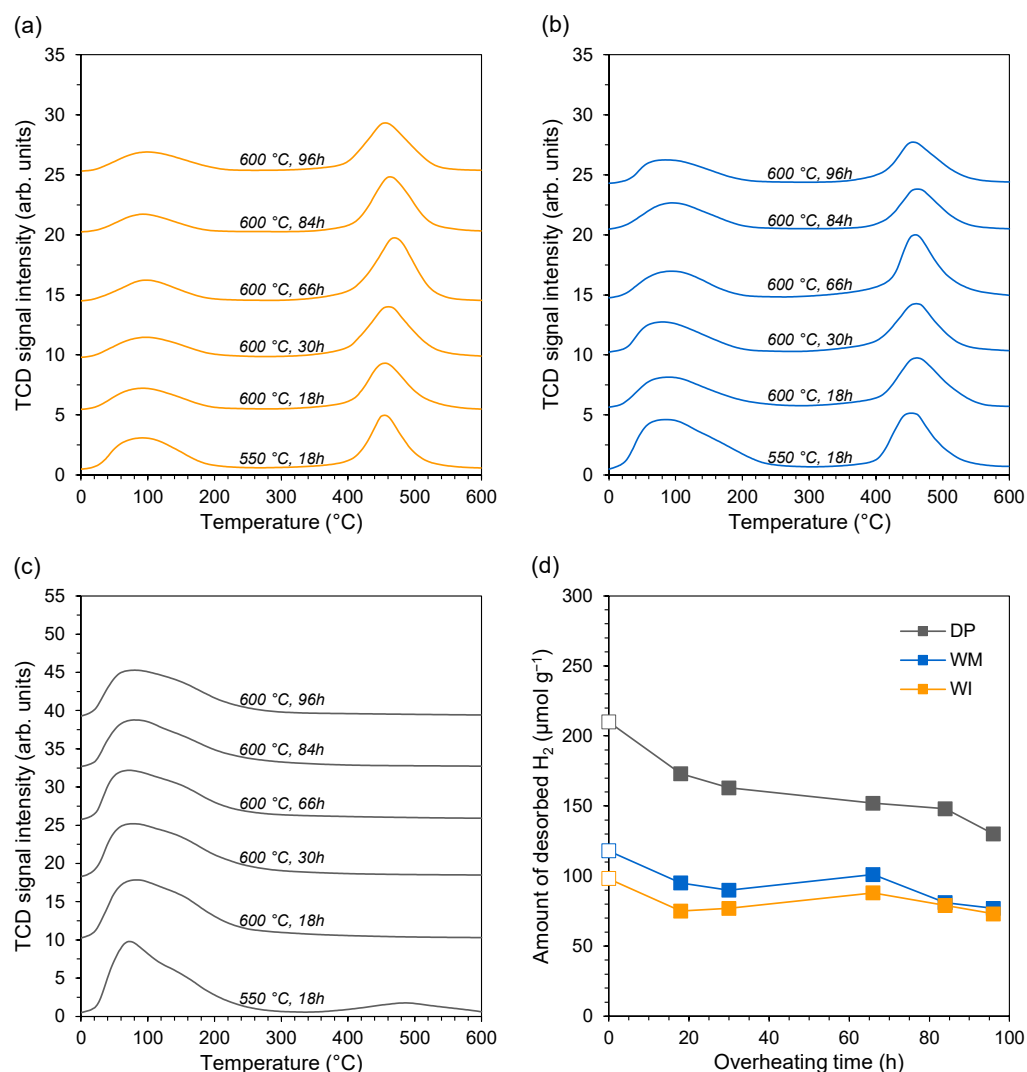


Figure 7. H₂-TPD profiles of the (a) WI catalyst, (b) WM catalyst, and (c) DP catalyst after reduction in hydrogen flow at 550 °C for 18 h and after overheating in hydrogen flow at 600 °C for 18, 30, 66, 84, and 96 h. (d) Changes in the amount of H₂ desorbed from the surface of the studied catalysts during long-term stability test.

The changes in the amount of desorbed H₂ from the surface of the tested catalysts during their long-term heat treatment are shown in Figure 7d. The observed trend of changes in the amount of desorbed H₂ is consistent with the observed slight changes in desorption profiles as a function of overheating time. For all the tested catalysts, the H₂ amount after overheating at 600 °C for 18 h decreased by ca. 20% compared to the amount desorbing after reduction at 550 °C for 18 h. Then, a slight decrease in the amount of desorbing hydrogen was observed during further long-term overheating at 600 °C, which finally, after 96 h, reached 3, 19, and 25% for WI, WM, and DP catalysts, respectively.

4. Discussion

It would seem that the most crucial feature of a catalyst is its activity. An equally, if not even more, critical feature for an industrial catalyst is its stability. The possibility of long-term operation of the catalyst in severe conditions of industrial processes without the need for regeneration or replacement is a basic requirement for their implementation. To fully assess the applicability of the catalyst, comprehensive characterization is required, including determination of its activity and investigation of its kinetic properties and stability of its operation under industrial conditions. The object of research presented in this paper was a cobalt catalyst promoted by cerium and barium for the ammonia synthesis process. As shown in our previous papers [30–32], this catalyst exhibits high activity in the NH_3 synthesis reaction, even several times higher than the activity of a commercial iron catalyst. However, the key point necessary to determine the possibility of its use in an industrial ammonia synthesis reactor is to determine its stability during long-term operation. The research described in this work aimed at determining the catalyst stability using the accelerated aging method, i.e., the only method that allows simulating in the laboratory the long-term catalyst operation in real reactor conditions. The obtained results helped us find the answer to the question about the factors determining changes in the activity of this catalyst during operation and indicate a potential mechanism for the deactivation of this catalyst.

Analyzing the results of the textural and structural characteristics of the catalyst, it can be concluded that the tested catalyst is highly resistant to high temperatures. The lack of significant changes in the size of the specific surface area (Table 1), morphology of the catalyst particles (Figure 3), distribution of elements on its surface (Figures 4–6), and chemisorption properties of the cobalt surface (Figure 7) during long-term heating at a temperature of 600 °C suggests that stable operation of the catalyst is possible in the ammonia synthesis reactor in the temperature range of 400–470 °C without the risk of losing its beneficial properties over time, which is confirmed by the data presented in Figure 1. However, the mechanism of catalyst deactivation by its slow sintering cannot be completely ruled out based on time-limited catalyst stability tests on a laboratory scale. Among the known mechanisms of catalyst deactivation, catalyst sintering seems to be the most likely cause of the loss of activity of a cobalt catalyst during its long-term operation, similar to a commercial fused iron catalyst. Despite its very high stability and exceptionally long lifespan (15 years or more), the Fe catalyst sinters slowly and requires periodic replacement. Important factors determining the lifespan of a cobalt catalyst are also resistance to poisoning, the possibility of regeneration in case of reversible poisoning (e.g., with oxygen compounds), and mechanical resistance. When comprehensively assessing the lifespan of a cobalt catalyst, it is necessary to consider poisoning tests and mechanical strength measurements for the formed catalyst.

The analysis of XRPD data draws attention to the presence of two crystalline forms of cobalt in the studied catalyst: hexagonal close-packed (hcp) and face-centered cubic (fcc). The proportion of these two phases changed when the catalyst was subjected to overheating at 600 °C, which was visible as a change in the intensity of reflections coming from these two phases (Figure 2). According to the literature [41–43], at a temperature of ca. 420 °C, a reversible hcp → fcc phase transformation occurs, i.e., at the temperature typical for the ammonia synthesis process. It is also known that the catalytic activity of cobalt in the ammonia synthesis reaction is strongly dependent on the form in which cobalt occurs in the catalyst [41]. The ability of N_2 and H_2 to adsorb on the cobalt surface depends on its phase. Hence, the NH_3 synthesis rates obtained for cobalt's hcp and fcc phases differ significantly. Rambeau's studies [41] showed that when conducting the process on cobalt with the hcp structure, the activity is twice as high as on cobalt with the fcc structure. Therefore, the hcp → fcc transformation is of particular importance in this case. The temperature of the ammonia synthesis process for a cobalt catalyst is close to the temperature of the hcp → fcc transformation of cobalt. Hence, this phenomenon may influence the efficiency of the NH_3 synthesis and the stability of catalyst operation at high temperatures over time.

The analysis of the obtained results also indicates that the method of introducing the Ba promoter does not impact the final properties, activity, and stability of the obtained CoCeBa catalyst. This is an extremely valuable observation from the point of view of the preparation of the tested catalyst. The introduction of the promoter is the last but crucial stage of catalyst synthesis. The presence of the Ba promoter in this catalyst is essential because it has an activating effect on cobalt and ensures good electron-donating properties of the catalyst surface required to conduct the NH_3 synthesis reaction effectively. The lack of a significant impact of the Ba addition method on the properties of the catalyst makes it possible to select the most appropriate method depending on the needs. Nowadays, much attention is paid to improving catalyst synthesis methods to achieve the highest possible activity of a given catalytic material in a specific process. Studies are focused on modifying synthesis methods, but more and more often turning into very complicated, sophisticated, and expensive methods that can be used to obtain small amounts of a highly active catalyst in a very time-consuming and/or energy-consuming process. However, the scale on which a given catalyst is to be finally used should always be considered. In the case of large-scale industrial processes, such as ammonia synthesis, a large amount of catalyst (several dozen tonnes) is required to be loaded into a single ammonia reactor. Hence, the catalyst production method should be relatively simple and easy to scale up. Considering the large-scale production of the CoCeBa catalyst for industrial purposes, the wet mixing method seems to be the most advantageous due to its simplicity and the lowest energy demand compared to other methods studied in this work (wet impregnation, deposition–precipitation).

5. Conclusions

Extended studies of the stability of the promoted cobalt catalyst for ammonia synthesis were carried out. The accelerated aging method was used to simulate the deterioration of catalyst performance during industrial operation. The catalyst was subjected to overheating for 436 h in a flow of a stoichiometric H_2/N_2 mixture at a temperature of 600 °C, i.e., a temperature much higher than the temperature of standard catalyst operation in the NH_3 synthesis reactor. The obtained results indicated that the CoCeBa catalyst is strongly resistant to overheating. The decline in catalyst activity during the long-term stability test was less than 10%. Textural and structural characteristics revealed the lack of significant changes in the specific surface area, morphology of the catalyst particles, and surface distribution of elements over time. Only a slight decrease in the amount of desorbed H_2 from the cobalt surface during their long-term heat treatment was observed. However, the nature of the adsorption sites on the catalyst surface did not change. The stable operation of the catalyst is possible in the ammonia synthesis reactor in the temperature range of 400–470 °C without the risk of losing its beneficial catalytic properties over time. The lack of a significant impact of the Ba addition method on the properties of the catalyst makes it possible to select the most appropriate method from the point of view of simplicity, costs, and energy consumption in the catalyst production process.

Supplementary Materials: The following supporting information can be downloaded at: <https://www.mdpi.com/article/10.3390/en16237787/s1>, Table S1: Physicochemical properties of the studied catalyst precursors; Table S2: Comparison of the catalytic performance for NH_3 synthesis of different catalysts; Table S3: Unit cell parameters and crystallite size of BaCeO_3 phase in the CoCeBa catalyst precursors; Table S4: Unit cell parameters and crystallite size of BaCeO_3 phase in the CoCeBa catalysts after overheating in H_2 (600 °C, 96 h). Figure S1: N_2 adsorption–desorption isotherms for (a) WI, (b) DP, (c) WM catalyst precursors obtained based on BJH adsorption isotherm model; Figure S2: Pore size distribution curves for (a) WI, (b) DP, (c) WM catalyst precursors obtained based on BJH adsorption isotherm model; Figure S3: XRPD patterns of the WI, DP, WM catalyst precursors; Figure S4: Arrhenius plots for the rate of ammonia synthesis at 6.3 MPa over the WI, DP, WM catalysts.

Author Contributions: Conceptualization, M.Z., H.R. and W.R.-P.; methodology, M.Z., H.R. and W.R.-P.; investigation, M.Z., H.R., W.P., W.R., A.O., K.S. and W.R.-P.; writing—original draft preparation, M.Z.; writing—review and editing, M.Z., H.R. and W.R.-P.; visualization, H.R. and K.S.; supervision, M.Z. All authors have read and agreed to the published version of the manuscript.

Funding: This research received no external funding.

Data Availability Statement: Data are contained within the article and supplementary materials.

Conflicts of Interest: The authors declare no conflict of interest.

References

1. Veziroglu, T.N.; Barbir, F. Hydrogen: The wonder fuel. *Int. J. Hydrogen Energy* **1992**, *17*, 391–404. [[CrossRef](#)]
2. Amin, M.; Shah, H.H.; Fareed, A.G.; Khan, W.U.; Chung, E.; Zia, A.; Farooqi, Z.U.; Lee, C. Hydrogen production through renewable and non-renewable energy processes and their impact on climate change. *Int. J. Hydrogen Energy* **2022**, *47*, 33112–33134. [[CrossRef](#)]
3. Singh, S.; Jain, S.; Ps, V.; Tiwari, A.K.; Nouni, M.R.; Pandey, J.K.; Goel, S. Hydrogen: A sustainable fuel for future of the transport sector. *Renew. Sustain. Energy Rev.* **2015**, *51*, 623–633. [[CrossRef](#)]
4. Nikolaidis, P.; Poullikkas, A. A comparative overview of hydrogen production processes. *Renew. Sustain. Energy Rev.* **2017**, *67*, 597–611. [[CrossRef](#)]
5. Jiang, L.-W.; Huang, Y.; Zou, Y.; Meng, C.; Xiao, Y.; Liu, H.; Wang, J.-J. Boosting the Stability of Oxygen Vacancies in α -Co(OH)₂ Nanosheets with Coordination Polyhedrons as Rivets for High-Performance Alkaline Hydrogen Evolution Electrocatalyst. *Adv. Energy Mater.* **2022**, *12*, 2202351. [[CrossRef](#)]
6. Wu, Y.Z.; Huang, Y.; Jiang, L.-W.; Meng, C.; Yin, Z.-H.; Liu, H.; Wang, J.-J. Modulating the electronic structure of CoS₂ by Sn doping boosting urea oxidation for efficient alkaline hydrogen production. *J. Colloid Interface Sci.* **2023**, *642*, 574–583. [[CrossRef](#)]
7. Huang, Y.; Jiang, L.-W.; Liu, H.; Wang, J.-J. Electronic structure regulation and polysulfide bonding of Co-doped (Ni, Fe)_{1+x}S enable highly efficient and stable electrocatalytic overall water splitting. *Chem. Eng. J.* **2022**, *441*, 136121. [[CrossRef](#)]
8. Acar, C.; Dincer, I. Review and evaluation of hydrogen production options for better environment. *J. Clean. Prod.* **2019**, *218*, 835–849. [[CrossRef](#)]
9. Lucentini, I.; Garcia, X.; Vendrell, X.; Llorca, J. Review of the Decomposition of Ammonia to Generate Hydrogen. *Ind. Eng. Chem. Res.* **2021**, *60*, 18560–18611. [[CrossRef](#)]
10. Lan, R.; Irvine, J.T.S.; Tao, S. Ammonia and related chemicals as potential indirect hydrogen storage materials. *Int. J. Hydrogen Energy* **2012**, *37*, 1482–1494. [[CrossRef](#)]
11. Klerke, A.; Christensen, C.H.; Nørskov, J.K.; Vegge, T. Ammonia for hydrogen storage: Challenges and opportunities. *J. Mater. Chem.* **2008**, *18*, 2304–2310. [[CrossRef](#)]
12. Berwal, P.; Kumar, S.; Khandelwal, B. A comprehensive review on synthesis, chemical kinetics, and practical application of ammonia as future fuel for combustion. *J. Energy Inst.* **2021**, *99*, 273–298. [[CrossRef](#)]
13. Herbinet, O.; Bartocci, P.; Grinberg Dana, A. On the use of ammonia as a fuel—A perspective. *Fuel Commun.* **2022**, *11*, 100064. [[CrossRef](#)]
14. Elbaz, A.M.; Wang, S.; Guiberti, T.F.; Roberts, W.L. Review on the recent advances on ammonia combustion from the fundamentals to the applications. *Fuel Commun.* **2022**, *10*, 100053. [[CrossRef](#)]
15. Valera-Medina, A.; Amer-Hatem, F.; Azad, A.K.; Dedoussi, I.C.; de Joannon, M.; Fernandes, R.X.; Glarborg, P.; Hashemi, H.; He, X.; Mashruk, S.; et al. Review on Ammonia as a Potential Fuel: From Synthesis to Economics. *Energy Fuels* **2021**, *35*, 6964–7029. [[CrossRef](#)]
16. Zhang, L.; Liang, J.; Wang, Y.; Mou, T.; Lin, Y.; Yue, L.; Li, T.; Liu, Q.; Luo, Y.; Li, N.; et al. High-Performance Electrochemical NO Reduction into NH₃ by MoS₂ Nanosheet. *Angew. Chem. Int. Ed.* **2021**, *60*, 25263. [[CrossRef](#)] [[PubMed](#)]
17. Liu, H. *Ammonia Synthesis Catalyst: Innovations and Practice*; World Scientific Publishing Co. Pte. Ltd.: Singapore; Chemical Industry Press: Beijing, China, 2013; pp. 686–705.
18. Hughes, R. *Deactivation of Catalysts*; Academic Press: London, UK, 1984.
19. Moulijn, J.A.; van Diepen, A.E.; Kapteijn, F. Catalyst deactivation: Is it predictable? What to do? *Appl. Catal. A Gen.* **2001**, *212*, 3–16. [[CrossRef](#)]
20. Argyle, M.D.; Bartholomew, C.H. Heterogeneous Catalyst Deactivation and Regeneration: A Review. *Catalysts* **2015**, *5*, 145–269. [[CrossRef](#)]
21. Bartholomew, C.H. Mechanisms of catalyst deactivation. *Appl. Catal. A Gen.* **2001**, *212*, 17–60. [[CrossRef](#)]
22. Bartholomew, C.H.; Farrauto, R.J. *Fundamentals of Industrial Catalytic Processes*, 2nd ed.; John Wiley & Sons, Inc.: Hoboken, NJ, USA, 2006.
23. Birtill, J.J. But will it last until the shutdown? Deciphering catalyst decay! *Catal. Today* **2003**, *81*, 531–545. [[CrossRef](#)]
24. Scott, S.L. A Matter of Life(time) and Death. *ACS Catal.* **2018**, *8*, 8597–8599. [[CrossRef](#)]
25. Pernicone, N. Methods for laboratory-scale evaluation of catalyst life in industrial plants. *Appl. Catal.* **1985**, *15*, 17–31. [[CrossRef](#)]

26. Liu, H.-Z.; Li, X.-N.; Hu, Z.-N. Development of novel low temperature and low pressure ammonia synthesis catalyst. *Appl. Catal. A* **1996**, *142*, 209–222. [[CrossRef](#)]
27. Pernicone, N.; Ferrero, F.; Rossetti, I.; Forni, L.; Canton, P.; Riello, P.; Fagherazzi, G.; Signoretto, M.; Pinna, F. Wustite as a new precursor of industrial ammonia synthesis catalysts. *Appl. Catal. A* **2003**, *251*, 121–129. [[CrossRef](#)]
28. Lin, B.; Guo, Y.; Lin, J.; Ni, J.; Lin, J.; Jiang, L.; Wang, Y. Deactivation study of carbon-supported ruthenium catalyst with potassium promoter. *Appl. Catal. A* **2017**, *541*, 1–7. [[CrossRef](#)]
29. Kowalczyk, Z.; Jodzis, S.; Raróg, W.; Zieliński, J.; Pielaszek, J. Effect of potassium and barium on the stability of a carbon-supported ruthenium catalyst for the synthesis of ammonia. *Appl. Catal. A* **1998**, *173*, 153–160. [[CrossRef](#)]
30. Raróg-Pilecka, W.; Karolewska, M.; Truszkiewicz, E.; Iwanek, E.; Mierzwa, B. Cobalt catalyst doped with cerium and barium obtained by Co-precipitation method for ammonia synthesis process. *Catal. Lett.* **2011**, *141*, 678–684. [[CrossRef](#)]
31. Karolewska, M.; Truszkiewicz, E.; Mierzwa, B.; Kępiński, L.; Raróg-Pilecka, W. Ammonia synthesis over cobalt catalysts doped with cerium and barium. Effect of the ceria loading. *Appl. Catal. A* **2012**, *445–446*, 280–286. [[CrossRef](#)]
32. Tarka, A.; Patkowski, W.; Zybert, M.; Ronduda, H.; Wicziński, P.; Adamski, P.; Sarnecki, A.; Moszyński, D.; Raróg-Pilecka, W. Synergistic Interaction of Cerium and Barium—New Insight into the Promotion Effect in Cobalt Systems for Ammonia Synthesis. *Catalysts* **2020**, *10*, 658. [[CrossRef](#)]
33. Kowalczyk, Z. Effect of potassium on the high-pressure kinetics of ammonia synthesis over fused iron catalysts. *Catal. Lett.* **1996**, *37*, 173–179. [[CrossRef](#)]
34. Lin, B.; Liu, Y.; Heng, L.; Wang, X.; Ni, J.; Lin, J.; Jiang, L. Morphology Effect of Ceria on the Catalytic Performances of Ru/CeO₂ Catalysts for Ammonia Synthesis. *Ind. Eng. Chem. Res.* **2018**, *57*, 9127–9135. [[CrossRef](#)]
35. Han, W.; Li, Z.; Liu, H. La₂Ce₂O₇ supported ruthenium as a robust catalyst for ammonia synthesis. *J. Rare Earths* **2019**, *37*, 492–499. [[CrossRef](#)]
36. Jafari, A.; Ebadi, A.; Sahebdehfar, S. Effect of iron oxide precursor on the properties and ammonia synthesis activity of fused iron catalysts. *Reac. Kinet. Mech. Cat.* **2019**, *126*, 307–325. [[CrossRef](#)]
37. Zhou, Y.; Ma, Y.; Lan, G.; Tang, H.; Han, W.; Liu, H.; Li, Y. A highly stable and active mesoporous ruthenium catalyst for ammonia synthesis prepared by a RuCl₃/SiO₂-templated approach. *Chin. J. Catal.* **2019**, *40*, 114–123. [[CrossRef](#)]
38. Zybert, M.; Karasińska, M.; Truszkiewicz, E.; Mierzwa, B.; Raróg-Pilecka, W. Properties and activity of the cobalt catalysts for NH₃ synthesis obtained by co-precipitation – the effect of lanthanum addition. *Pol. J. Chem. Technol.* **2015**, *17*, 138–143. [[CrossRef](#)]
39. Lin, B.; Liu, Y.; Heng, L.; Ni, J.; Lin, J.; Jiang, L. Effect of barium and potassium promoter on Co/CeO₂ catalysts in ammonia synthesis. *J. Rare Earths* **2018**, *36*, 703–707. [[CrossRef](#)]
40. Ronduda, H.; Zybert, M.; Patkowski, W.; Sobczak, K.; Moszyński, D.; Albrecht, A.; Sarnecki, A.; Raróg-Pilecka, W. On the effect of metal loading on the performance of Co catalysts supported on mixed MgO–La₂O₃ oxides for ammonia synthesis. *RSC Adv.* **2022**, *12*, 33876–33888. [[CrossRef](#)]
41. Rambeau, G.; Jorti, A.; Amarglio, H. Catalytic activity of a cobalt powder in NH₃ synthesis in relation with the allotropic transformation of the metal. *J. Catal.* **1985**, *94*, 155–165. [[CrossRef](#)]
42. Ray, A.E.; Smith, S.R.; Scofield, J.D. Study of the phase transformation of cobalt. *Phase Equilib.* **1991**, *12*, 644–647. [[CrossRef](#)]
43. Matsumoto, H. Shift of $\alpha \rightarrow \beta$ transformation temperature of cobalt with thermal cycling. *J. Mater. Sci. Lett.* **1993**, *12*, 969–970. [[CrossRef](#)]
44. Ronduda, H.; Zybert, M.; Patkowski, W.; Moszyński, D.; Albrecht, A.; Sobczak, K.; Małolepszy, A.; Raróg-Pilecka, W. Co nanoparticles supported on mixed magnesium–lanthanum oxides: Effect of calcium and barium addition on ammonia synthesis catalyst performance. *RSC Adv.* **2023**, *13*, 4787–4802. [[CrossRef](#)] [[PubMed](#)]
45. Schlögl, R. Catalytic Synthesis of Ammonia—A “Never-Ending Story”? *Angew. Chem. Int. Ed.* **2003**, *42*, 2004–2008. [[CrossRef](#)] [[PubMed](#)]
46. Humphreys, J.; Lan, R.; Tao, S. Development and Recent Progress on Ammonia Synthesis Catalysts for Haber–Bosch Process. *Adv. Energy Sustain. Res.* **2021**, *2*, 2000043. [[CrossRef](#)]
47. Ertl, G. Reactions at Surfaces: From Atoms to Complexity (Nobel Lecture). *Angew. Chem. Int. Ed.* **2008**, *47*, 3524–3535. [[CrossRef](#)] [[PubMed](#)]
48. Cao, A.; Bukas, V.J.; Shadravan, V.; Wang, Z.; Li, H.; Kibsgaard, J.; Chorkendorff, I.; Nørskov, J.K. A spin promotion effect in catalytic ammonia synthesis. *Nat. Commun.* **2022**, *13*, 2382. [[CrossRef](#)]
49. Ertl, G. Elementary steps in ammonia synthesis: The surface approach. In *Catalytic Ammonia Synthesis. Fundamentals and Practice*, 1st ed.; Jennings, J.R., Ed.; Springer Science+Business Media: New York, NY, USA, 1991; pp. 109–132.
50. Ronduda, H.; Zybert, M.; Patkowski, W.; Tarka, A.; Jodłowski, P.; Kępiński, L.; Sarnecki, A.; Moszyński, D.; Raróg-Pilecka, W. Tuning the catalytic performance of Co/Mg–La system for ammonia synthesis via the active phase precursor introduction method. *Appl. Catal. A* **2020**, *598*, 117553. [[CrossRef](#)]
51. Ronduda, H.; Zybert, M.; Dziewulska, A.; Patkowski, W.; Sobczak, K.; Ostrowski, A.; Raróg-Pilecka, W. Ammonia synthesis using Co catalysts supported on MgO–Nd₂O₃ mixed oxide systems: Effect of support composition. *Surf. Interfaces* **2023**, *36*, 102530. [[CrossRef](#)]

Disclaimer/Publisher’s Note: The statements, opinions and data contained in all publications are solely those of the individual author(s) and contributor(s) and not of MDPI and/or the editor(s). MDPI and/or the editor(s) disclaim responsibility for any injury to people or property resulting from any ideas, methods, instructions or products referred to in the content.